Qualitative Visual Comparison of Three Simulations of Fluid Flow around a Flying Bat

Mykhaylo Kostandov
mk@cs.brown.edu

Sc.M. project introduction

My work on this project, supervised by Professor David H. Laidlaw, is described in the attached paper. The main focus of the paper is on the qualitative comparison and analysis of flow features produced by two existing computational fluid dynamics (CFD) approaches, NekTar and FastAero, and the relationship of simulation parameters to the experimental context.

The paper was a result of a joint collaboration with several coauthors with different expertise. I drove most of the work on the project; in particular, I reviewed and analyzed related work, designed and implemented the previsualization pipeline and visualization techniques, created all the videos and images using these techniques, and wrote the paper. Acquisition of the experimental kinematics data was done by members of the Swartz bat flight research group. Fluid flow simulations from the two approaches were also completed previously. Some interpretation and analysis of the results was done in collaboration with the coauthors, as described below.

Dr. David J. Willis served as the aerodynamics expert and provided his knowledge of CFD methods and model assumptions; he was also actively involved in describing the expectations of method performance in the context of viscosity modeling (in particular, Section 3.1). Dr. Igor V. Pivkin was previously working on creating visualizations of NekTar simulation data and integrating the NekTar simulator interface library into the visualization group's software framework. Dr. Sharon M. Swartz served as the evolutionary biology expert on my committee. Dr. David H. Laidlaw, as my research advisor, provided guidance in designing and analyzing the visualizations and reviewed the manuscript.

Student Signature

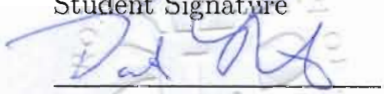

Advisor Signature

5/7/08

Date

Qualitative Visual Comparison of Three Simulations of Fluid Flow around a Flying Bat

Mykhaylo Kostandov, *Student Member, IEEE*, David J. Willis, Igor V. Pivkin,
Sharon M. Swartz, and David H. Laidlaw, *Senior Member, IEEE*

Abstract—
We present a case study in using scientific visualization techniques to qualitatively explore predicted flow fields generated by bats in flight, which resulted in a better insight into methods for studying aerodynamic behavior of bats. Our study involved a qualitative comparison of flow features derived from both Navier-Stokes computations and potential flow computational aerodynamics models. As a result of using visual representations of simulated flow structures for various tasks, we characterized the effect of surface model approximation order on vortex formation in the wake model, compared the complexity of the resulting structures, and compiled a set of wake characteristics. By establishing a visual connection between bat wing kinematics and dominant flow structures, we provided a way to explore and discover correlations between wing motion and flow behavior. Advantages and drawbacks of visualization methods and flow modeling factors are also discussed in the context of a higher-fidelity Navier-Stokes simulation model, a lower-fidelity potential flow computational aerodynamics model, and experimental settings.

Index Terms—Scientific visualization, flow visualization, computational methods, visual analysis, modeling in natural sciences.

1 Introduction

Visualization of fluid dynamics simulation data is one of the ubiquitous driving problems in scientific visualization. Effective visualizations can provide much-needed help to scientists who study natural phenomena in an environment that facilitates generation, evaluation, and refinement of scientific hypotheses and insight. We describe the lessons learned in the development process of such visualizations, which were created in collaboration with bat flight researchers and intended to enhance the transfer of scientific knowledge and to provide new ways to understand the aerodynamic behavior of flying animals.

The simulations used high-resolution experimental data derived from stereo photogrammetric techniques applied to bats flying in a controlled space. The only flying mammals, bats (Order Chiroptera) provide an excellent example of a highly complex animal locomotor apparatus, which is employed in spatially and temporally convoluted ways. The unique features of bats – their specialized skeletal anatomy, high muscular control over wing conformation, and highly deformable wing-membrane – yield wings that undergo large changes in 3D geometry with every wingbeat cycle, and consequently produce highly maneuverable and energetically efficient flight patterns [27, 29, 30, 31, 32, 33, 38].

Correct models of such complex flight have the potential to foster significant new discoveries in the biological evolution of flight. These models may also provide insight useful for engineering biologically-inspired micro air vehicles (MAVs) [3, 5, 15, 23] with increased maneuverability and in-flight sensing capabilities. To more fully understand flight, one first needs to understand and characterize the fluid structures produced by the the motion of wings in flight. This can be achieved using computational models of flow, from which one can derive and analyze aerodynamic forces, connection between kinematics and flow dynamics, etc.

Wakes in flying animals have been described, visualized, and characterized in experimental-domain work [4, 6, 8, 18, 24, 25, 34, 37]. Computational fluid dynamics simulations are commonly used in studies of insect flight [12, 13, 17, 28]. In particular, a recent study of insect hovering flight [2] used a Navier-Stokes CFD solver and provided an integrative computational study of unsteady wake dynamics in a fruit fly. In the study, Reynolds number Re=134, and the body mass of a fruit fly is sufficiently small, so a traditional low-Re Navier-Stokes method provides a realistic model of the experimental data. However, for a much larger animal, such as a bat, the requirements for lift and thrust, as well as the Re number, are significantly more challenging.

In this study, we focus on results from two distinctly different approaches to simulating fluid flow around the flapping wing. The higher-fidelity computational approach, NekTar [10], is a hybrid spectral/hp element high-order incompressible Navier-Stokes method, which uses an unstructured tetrahedral mesh. The lower-fidelity approach, FastAero [35], is an accelerated potential flow boundary element method. FastAero uses a vortex particle representation of the wake and does not take viscous effects into account, so there is no separation model, no viscous drag, and no dissipation of the flow structures. It should be noted that the simulation data discussed in this paper was not available for the same experimental wing geometry, so datasets used for NekTar and FastAero came from different experimental cases.

Although we can use insight gained in other aerodynamics studies, such as fixed wing aircraft and flapping rigid wings, to indicate regions, which likely contain flow features of interest, the detailed flow structures in unsteady flapping wing flight are not known a priori. Some of these regions of interest are wake structures and near- and far-field flow behavior.

Ultimately, our goal is to construct a set of analysis methods that can tell us what is happening in the wake. It is desirable that these methods work across multiple data types and datasets, so different simulation approaches can be evaluated using the same analytical pipeline. However, we also want deeper understanding of flow structures within a single simulation approach, and some attributes and methods might be simulation-specific (e.g. the vortex particle wake produced by FastAero). In this paper, we describe our exploration of the simulation data and discuss lessons learned.

- *Mykhaylo Kostandov and David H. Laidlaw are with the Computer Science Department, Brown University, Providence, RI 02912, E-mail: {mk, dhl}@cs.brown.edu.*
- *David J. Willis is with the Division of Engineering, Brown University, Providence, RI 02912, and with the Department of Aeronautics and Astronautics, Massachusetts Institute of Technology, Cambridge, MA 02139, E-mail: djwillis@mit.edu.*
- *Igor V. Pivkin is with the Division of Applied Mathematics, Brown University, Providence, RI 02912, E-mail: piv@cfm.brown.edu.*
- *Sharon M. Swartz is with the Department of Ecology and Evolutionary Biology, Brown University, Providence, RI 02912, E-mail: Sharon_Swartz@brown.edu.*

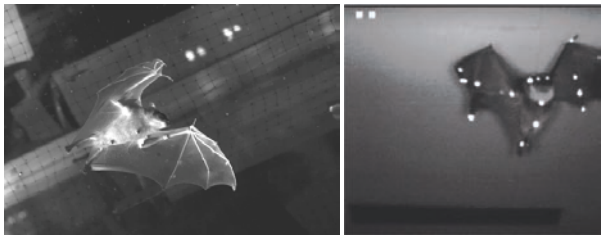

Fig. 1. Frames from wind tunnel videos recorded by high-speed digital cameras. Left: *Cynopterus brachyotis*, used in FastAero simulations. Right: *Pteropus Poliocephalus*, used in NekTar simulations. The 3D coordinates of markers attached to the bat wings are reconstructed using Direct Linear Transformation.

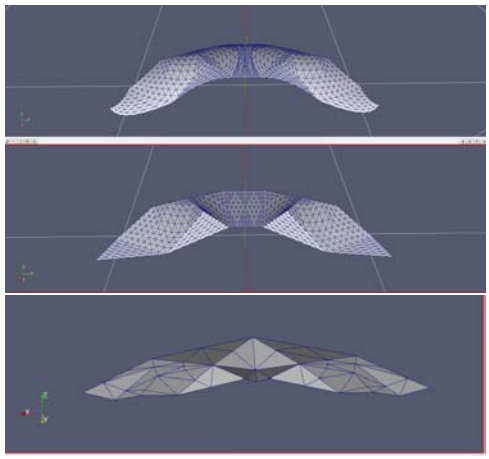

Fig. 2. Preprocessed geometrical models of the wing surface used in the three simulations. Top to bottom: higher-order geometry models ("curved" and "sharp" wings) used in FastAero, and the lower-order "sharp" model used in NekTar.

2 METHODS

In our study, we concentrated on using visualization techniques to explore and characterize the simulation results. After wind tunnel capture and preliminary data processing, bat wing models were constructed and used as inputs into the computational fluid dynamics tools. A set of common visualization techniques was applied to the results of CFD processing, including time-varying flow field data in the format common to all the datasets, as well as simulation-specific data, such as the FastAero vortex particle wake.

2.1 Kinematic acquisition and preprocessing

Experimental bat wing kinematics data were acquired by flying a bat in a wind tunnel [29] at different speeds determined by the air flow speed set in the tunnel. Three high-speed digital cameras (data used for FastAero was collected at f=1000Hz, and for NekTar at f=500Hz) tracked the positions of painted markers attached to bone joints and wing membranes during steady forward flight (Fig. 1). The image data was extracted [9] and converted into a set of 3D marker coordinates using Direct Linear Transformation (DLT) [1]. A detailed description of postprocessing steps that addressed experimental issues such as missing data points, high-frequency noise, and others, before constructing the meshes for the simulation, is provided in [19].

NekTar simulation used a low-order "sharp wing" geometrical model (see Fig. 2). In FastAero, two geometrical models were constructed using the same set of captured kinematics – a "curved wing" model using the full set of markers (bone and wing), and a "sharp wing" model that used a smaller subset of markers. A detailed description of wing mesh construction for FastAero using quadratic surface patches and an inertial model of the wing is provided in [36].

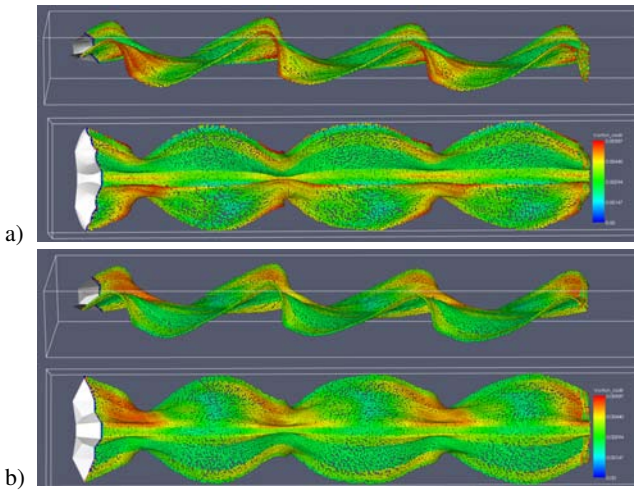

Fig. 3. FastAero, beginning of a downstroke. a) curved wing and b) sharp wing, vortex particles colored by vortex particle radii.

2.2 Flow simulation datasets

NekTar simulation used a kinematics dataset of a gray-headed flying fox (*Pteropus Poliocephalus*). The simulation used a mean flight speed v_f=1 m/s and Re=10.

FastAero simulations used data from experiments with a lesser short-nosed fruit bat (*Cynopterus brachyotis*). Mean flight speed used in the simulator was v_f=4.79 m/s. As FastAero uses an inviscid model, it is independent of Re.

The relationship of simulation parameters to those characteristic of real flow is discussed in Section 3.4.

2.3 Frames of Reference

Air frame of reference (AFR) is the frame affixed to the undisturbed air. Body frame of reference (BFR) moves with the forward flying speed of the bat; to obtain velocity field values in AFR, we subtract free flow velocity from the BFR field produced by the simulations. As the free flow velocity component aligned with the direction of motion is usually considerably larger than the velocity field components in the transverse plane, exploring the field in AFR helps highlight the disturbance caused by the wing. Effectively, as BFR velocity field represents the behavior of steady incoming flow interacting with a flapping wing fixed in space, AFR velocity field represents the behavior of a flapping wing moving through previously static air.

2.4 Visualization techniques

Visualization of preprocessed flow data was done using ParaView [26], a widely used open-source VTK-based visualization package. Given the differences in the simulation source data, we replicated data processing and visualization setup across datasets as closely as possible in order to compare the results. For most tasks, a single wingbeat was separated in each dataset, and flow behavior was qualitatively analyzed at characteristic time snapshots along the up- and downstroke.

2D cutting planes are among the most common tools used to explore the velocity field data. We used planes to display color-coded interpolated magnitude values of velocity in BFR domain ($\vec{v}_{BFR}$), velocity in AFR domain ($\vec{v}_{AFR}$), and vorticity ($\vec{\omega}$). Although free positioning of the plane is allowed, preferred slicing direction is usually in spanwise and transverse planes, which are most commonly used in experimental studies of flow behavior around the flapping wing. We also augmented planes with arrow glyphs to show the plane surface vectors of the sampled velocity field, as well as isocontours of the scalar magnitude values.

In addition to planes, streamtubes through the velocity field were used, usually color-mapped to velocity or vorticity values. Fig. 4 shows streamtubes of v_{BFR} field, colored by vorticity magnitude, and

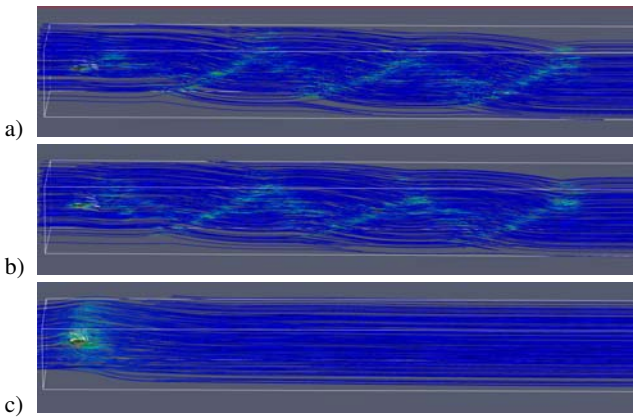

Fig. 4. Beginning of a downstroke. a) and b) v_{BFR} streamtubes in FastAero (curved and sharp wing), and c) in NekTar, colored by vorticity magnitude $|\vec{\omega}|$.

Fig. 5 shows streamtubes of v_{AFR} field, colored by the logarithm of the vorticity magnitude.

In related work, NekTar-simulated airflow around bat wings was visualized with animated streamlines and pathlines [16, 21], but in this study we focus on manual comparison of time-varying data frame by frame.

FastAero represents the wake shed by the wing using a vortex particle approach [35], which allows for rapid automatic generation of vorticity in the domain. We represent vortex particles (present only in FastAero) with spherical glyphs in 3D space (see Fig. 3).

3 Results and Discussion

In this section, we talk about the lessons we have learned from using visualizations to analyze different approaches, such as comparing the wake behavior predicted by FastAero and NekTar, choosing the order of wing geometry used in the FastAero simulation, discussing implications for experimental design, and analyzing the simulation parameters in the context of known parameters of real flows. We also illustrate how visualization techniques helped facilitate the process by highlighting features of interest depending on the exploration task.

3.1 Solver characteristics and simulation results

The dominant difference between NekTar and FastAero methods is that physics-wise the NekTar code has viscous losses while FastAero does not. As a result, NekTar can predict separation, and FastAero can not. This also means that when a NekTar simulation uses a lower *Re* regime than the real flow, it will predict larger boundary layers and viscous layers. These are the types of points of interest and difference we expect, and the question is how much these effects change the results we see. Consistencies between the models, within reason, would provide good indication that models partly predict real behavior.

NekTar is a high order spectral element code for solving Navier-Stokes equations in laminar flow regimes. The model described here was computed at *Re*=10. This low *Re* means that the physical structures in the flow will dissipate much more rapidly than actually happens in flight (at *Re* above 40×10^3). The effects of viscosity can be seen when comparing spanwise (Fig. 9 for v_{BFR} and Fig. 10 for v_{AFR}) and transverse (Fig. 11) cutting planes. Wake structures, especially smaller vortices, are expected to dissipate rapidly in this model and do not provide large amounts of insight into wake structures, unless the data is forced to persist as a time history. Also, viscous effects (boundary layer thickness, separation and reattachment lines and locations), though present, may not represent the characteristics of the actual *Re* number regime that is considered. This is worrisome since it means that the cost is high and the lack of model matching (through *Re*) means that the solution is not easily trusted.

FastAero, on the other hand, is a potential solver that uses an inviscid model. As a result, there is no dependence on *Re* number, and flow

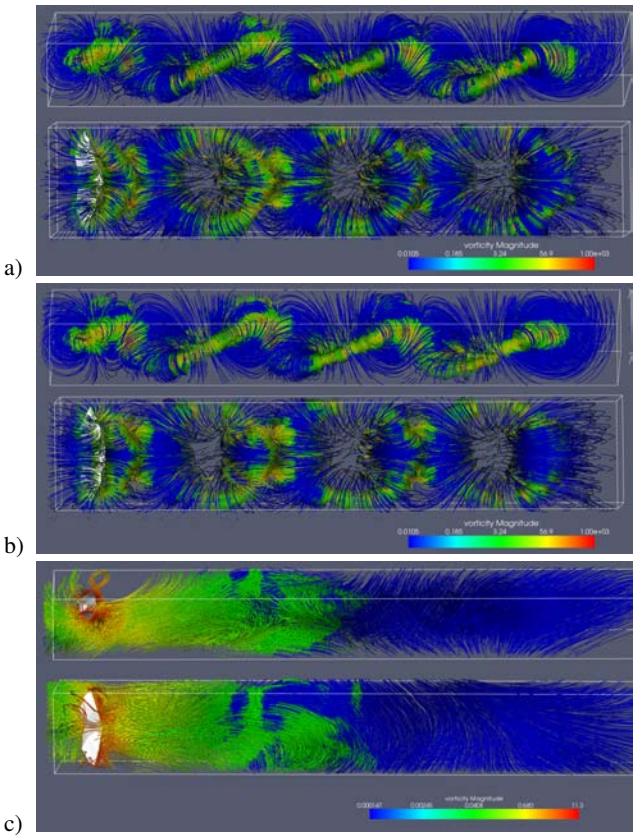

Fig. 5. Beginning of a downstroke. a) and b) v_{AFR} streamtubes in FastAero (curved and sharp wing), and c) in NekTar, colored by $log|\vec{\omega}|$.

structures do not dissipate or get destroyed, as illustrated in spanwise (Fig. 9 for v_{BFR} and Fig. 10 for v_{AFR}) and transverse (Fig. 11) cutting planes. Separation is not predicted in the model, but if the flow leaves the wing in an attached state, the model may be predictive. That is, if there is separation and subsequent reattachment, such as in a leading-edge vortex, one might get a reasonable prediction even though some features are not well represented).

A close-up of streamtubes through AFR velocity domain (Fig. 6) shows the effects of wing bound circulation and wake vorticity at leading and trailing edges.

3.2 The effect of wing geometry features on generated flow

By comparing simulation results from high- and low-order geometrical models, we seek to find out how the domain reacts to different approximations of the wing surface. The question is whether it is acceptable to use a lower approximation (for example, by using less markers) without sacrificing the validity of the observed simulation results. Theoretically, we would expect sharp corners in wing geometry to create stronger and physically unrealistic vortex structures in the wake.

Looking at the snapshots of flow field from curved and sharp wing cases at the same timesteps (Fig. 9 and Fig. 10), we can see the formation of high-velocity regions above the wing and low-velocity regions below the wing, creating lift forces necessary to support the body. By following the time snapshots, we can observe these regions shedding into the wake. A mid-body spanwise slicing plane (Fig. 7) also shows a far-field snapshot of the wake produced by multiple wingbeats.

3.3 Region-of-interest (ROI) suggestion for experimental DPIV

Digital particle image velocimetry (DPIV) is one of the increasingly common experimental tools [7, 11, 14, 25, 22], which provides instan-

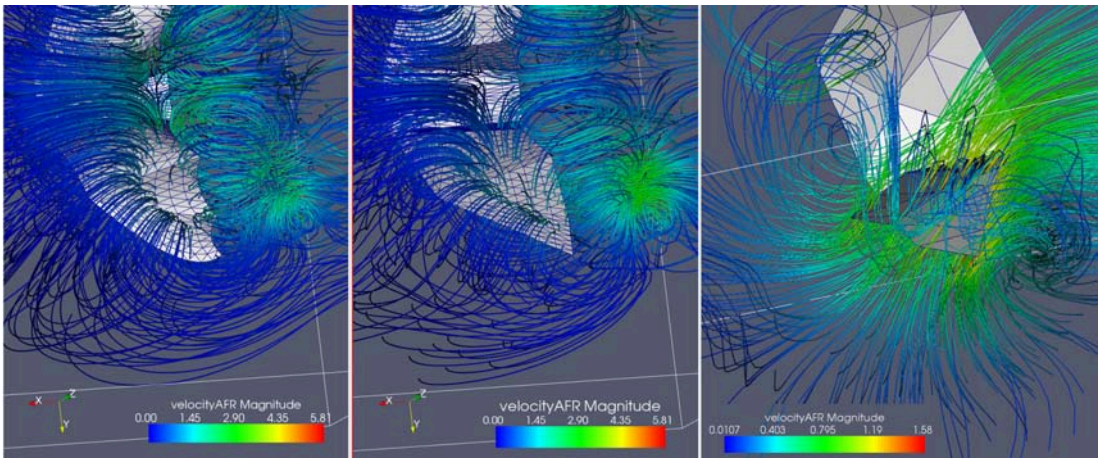

Fig. 6. v_{AFR} streamtubes in 3 cases (curved FastAero, sharp FastAero, and NekTar) in mid-downstroke. In both FastAero cases the streamtubes illustrate the effects of wing bound circulation and wake vorticity at leading and trailing edges.

taneous velocity vector measurements in a cross-section of the flow. Biologists and aerodynamics experts are used to looking at DPIV-type slices to get understanding of the flow behavior. "Virtual DPIV" seems like a good way to present exploration options in a simulation environment, as well as lay down the framework for integrating experimental and simulation data together.

Effectively, the cutting planes we have used earlier in the paper emulate DPIV acquisition process for a simulated flow domain. By exploring predicted behavior throughout the domain, ROI for real plane positioning can be determined. This streamlines the DPIV window positioning process and allows more effective data collection by reducing tedious trial-and-error experimental positioning.

3.4 Relationship to experimental setting

As we know, $Re = \rho v_f L/\mu$, where ρ is the fluid density, v_f is the mean fluid velocity, L is the characteristic length (average chord in this case), and μ is the dynamic fluid viscosity. As a consequence, the size of the bat and the forward speed are important in defining the *Re* range. For example, a recent experimental study [7] used DPIV in a low-turbulence tunnel to analyze wakes produced in flapping flight of Pallas's long-tongued bat (*Glossophaga soricina*) at speeds from 1.5 to 7 m/s and $Re \approx 4\times10^3$ to 18×10^3. A follow-up study [14] of leading-edge vortices in these wakes used flight speed of 1 m/s and $Re \approx 5\times10^3$. While the aforementioned studies used *G. soricina* with the body mass of 11g, the simulations we have described in this paper used data from larger animals, *Cynopterus brachyotis* (body mass of 35g, typical mass range of 30-100g) and *Pteropus Poliocephalus* (average body mass of 677 g, mass range of 600-1000g), so *Re* is higher in our case. Typical *Re* ranges are considered to be $Re \approx 12\times10^3$ to 40×10^3 for *C. brachyotis*, and greater than 40×10^3 for *P. Poliocephalus*.

However, the NekTar dataset used in this paper was simulated at $Re = 10$, which is more than 3 orders of magnitude below the experimental range for *P. Poliocephalus* bats. Computational results being significantly below real flight regime makes it impossible to make judgments about flight mechanisms of the real bat. FastAero, on the other hand, uses an inviscid model (so *Re* approaches infinity), which is not a physically exact approximation of real flight either, but can provide more valuable insight into flow behavior in cases where viscous effects are expected to be manifested weakly. It would also be useful to look at different forward flight velocities in addition to *Re*, since the lift and thrust requirements will be different (for example, a fast-flying small bat and a slow-flying large bat might fly at the same *Re* but exhibit completely different force strategies.

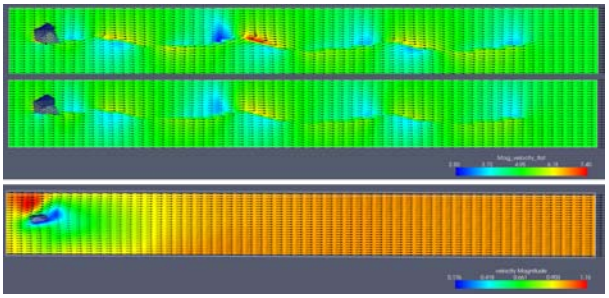

Fig. 7. Overview of v_{BFR} vectors and contours in FastAero (curved and sharp geometry) and NekTar. Color maps are different between the two cases; cutting plane is located at mid-body. Viscous effects are clearly manifested in the NekTar case.

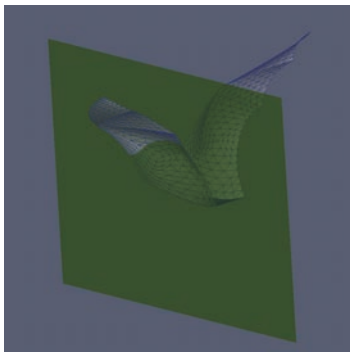

Fig. 8. The position of the spanwise cutting plane used in Fig. 9 and Fig. 10.

4 Conclusion

In this paper, we focused on exploring simulation results from two simulations of fluid flow around a model of the flapping bat wing, ob-

tained from experimental flight data. We used visualizations of simulation data to explore the behavior of predicted wakes and to explore the advantages and disadvantages of each method, as well as the significance of simulation parameters, such as the order of wing geometry approximation, within one method. The expectations of flow behavior differences due to the assumptions that the methods made about the viscosity model were supported.

As *Re* number currently used in NekTar simulations is far from reality, effectively this model should not be recommended to make conclusions about. By design, this results in predicting larger boundary layers and viscous layers. We expect that FastAero, although not modeling viscous forces, would be a lot closer to the truth and more useful as an exploratory model. Depending on the near-wing flow structures, FastAero may prove to be a good model for rapidly investigating bat flight and providing some insight into the flow field. The lack of a viscous model, however, limits the prediction of flow separation, the presence of leading edge vortices and viscous drag, all of which may play a critical role in bat flight. If bats do indeed maintain a predominantly attached flow during flight, which is more likely at faster speeds rather than hovering speeds, the use of FastAero is more fully justified.

Eventually, to validate computational fluid dynamics models, a comparison with data from experimental flight must be made, such as in [20, 39], and others. To our knowledge, no study of bat flight to date has combined experimentally measured velocity field measurements, such as DPIV, with flow models based on real body and wing kinematics. We believe this should be a necessary step in analyzing computational models, and it is important to point out that the parameters used for models should be reasonably correlated with known parameters of flight.

REFERENCES

[1] Y. Abdel-Aziz and H. Karara. Direct linear transformation from comparator coordinates into object space coordinates in close-range photogrammetry. *Proc. of the Symposium on Close-Range Photogrammetry*, pages 1–18, January 1971.

[2] H. Aono, F. Liang, and H. Liu. Near-and far-field aerodynamics in insect hovering flight: an integrated computational study. *J. Exp. Bio.*, 211(2):239, 2008.

[3] F. J. Boria, R. Bachmann, P. Ifju, R. Quinn, R. Vaidyanathan, C. Perry, and J. Wagener. A sensor platform capable of aerial and terrestrial locomotion. *Proc. IROS 2005*, pages 3959–3964, 2005.

[4] M. H. Dickinson, F. Lehmann, and S. Sane. Wing rotation and the aerodynamic basis of insect flight. *Science*, 284(5422):1954–1960, 1999.

[5] C. Ellington. The novel aerodynamics of insect flight: Applications to micro-air vehicles. *Journal of Experimental Biology*, 202(23):3439–3448, 1999.

[6] C. P. Ellington. Leading-edge vortices in insect flight. *Nature*, 384(6610):626–630, 1996.

[7] A. Hedenström, L. Johansson, M. Wolf, R. von Busse, Y. Winter, and G. Spedding. Bat flight generates complex aerodynamic tracks. *Science*, 316(5826):894, 2007.

[8] A. Hedenström, M. Rosén, and G. Spedding. Vortex wakes generated by robins erithacus rubecula during free flight in a wind tunnel. *J. Royal Soc. Interface*, 3(7):263–276, 2006.

[9] T. L. Hedrick. Matlab tools for digitizing video files and calibrating cameras. http://www.unc.edu/∼thedrick/software1.html, 2007.

[10] G. E. Karniadakis and S. J. Sherwin. *Spectral/hp element methods for computational fluid dynamics*. Oxford University Press, Oxford, 2005.

[11] G. Lauder and E. Drucker. Morphology and experimental hydrodynamics of fish fin control surfaces. *IEEE J. of Oceanic Engineering*, 29(3):556–571, 2004.

[12] H. Liu and K. Kawachi. A numerical study of insect flight. *J. Comp. Physics*, 146(1):124–156, 1998.

[13] L. Miller and C. Peskin. A computational fluid dynamics of 'clap and fling'in the smallest insects. *J. Exp. Bio.*, 208(2):195–212, 2005.

[14] F. T. Muijres, L. C. Johansson, R. Barfield, M. Wolf, G. R. Spedding, and A. Hedenström. Leading-edge vortex improves lift in slow-flying bats. *Science*, 319(5867):1250, 2008.

[15] D. Page. Micro-air-vehicles: Learning from birds and bees. *High Technology Careers Magazine*, 2001.

[16] I. Pivkin, E. Hueso, R. Weinstein, D. H. Laidlaw, S. Swartz, and G. Karniadakis. Simulation and visualization of air flow around bat wings during flight. In *Proceedings of International Conference on Computational Science*, pages 689–694, 2005.

[17] R. Ramamurti and W. Sandberg. A three-dimensional computational study of the aerodynamic mechanisms of insect flight. *J. Exp. Bio.*, 205(10):1507–1518, 2002.

[18] J. Rayner, G. Jones, and A. Thomas. Vortex flow visualizations reveal change in upstroke function with flight speed in bats. *Nature*, 321(6066):162–164, 1986.

[19] D. K. Riskin, D. J. Willis, J. Iriarte-Diaz, T. L. Hedrick, M. Kostandov, J. Chen, D. H. Laidlaw, K. S. Breuer, and S. M. Swartz. Quantifying the complexity of bat wing kinematics. *J. Theor. Bio.*, 2008. In Review.

[20] Q. Shen. Comparisons of wind tunnel experiments and computational fluid dynamics simulations. *J. Visualization*, 6(1):31–39, 2003.

[21] J. S. Sobel, A. S. Forsberg, D. H. Laidlaw, R. C. Zeleznik, D. F. Keefe, I. Pivkin, G. E. Karniadakis, P. Richardson, and S. Swartz. Particle flurries: Synoptic 3D pulsatile flow visualization. *IEEE CG&A*, 24(2):76–85, 2004.

[22] G. Spedding, A. Hedenstrom, and M. Rosen. Quantitative studies of the wakes of freely flying birds in a low-turbulence wind tunnel. *Experiments in Fluids*, 34(2):291–303, 2003.

[23] G. Spedding and P. Lissaman. Technical aspects of microscale flight systems. *Journal of Avian Biology*, 29(4):458–468, 1998.

[24] G. R. Spedding, J. M. V. Rayner, and C. J. Pennycuick. Momentum and energy in the wake of a pigeon (columba livia) in slow flight. *J. Exp. Bio.*, 111(1):81–102, 1984.

[25] G. R. Spedding, M. Rosen, and A. Hedenstrom. A family of vortex wakes generated by a thrush nightingale in free flight in a wind tunnel over its entire natural range of flight speeds. *The Journal of Experimental Biology*, 206:2313–2344, 2003.

[26] A. Squillacote. *The ParaView Guide*. Kitware, 2006.

[27] E. Stockwell. Morphology and flight manoeuvrability in new world leaf-nosed bats (chiroptera : Phyllostomidae). *Journal of Zoology*, 254:505–514, 2001.

[28] M. Sun and J. Tang. Unsteady aerodynamic force generation by a model fruit fly wing in flapping motion. *J. Exp. Bio.*, 205(1):55–70, 2002.

[29] S. Swartz, K. Bishop, and M. Ismael-Aguirre. Dynamic complexity of wing form in bats: Implications for flight performance. *Functional and Evolutionary Ecology of Bats*, 2006.

[30] S. Swartz, P. Freeman, and E. Stockwell. Ecomorphology of bats: comparative and experimental approaches relating structural design to ecology. *Bat Ecology*, 2003.

[31] S. M. Swartz, M. D. Groves, H. D. Kim, and W. R. Walsh. Mechanical properties of bat wing membrane skin: aerodynamic and mechanical functions. *Journal of Zoology*, 239:357–378, 1996.

[32] X. Tian, J. Iriarte, K. Middleton, R. Galvao, E. Israeli, A. Roemer, A. Sullivan, A. Song, S. Swartz, and K. Breuer. Direct measurements of the kinematics and dynamics of bat flight. In *Proceedings of 36th AIAA Fluid Dynamics Conference*, June 2006.

[33] C. Voigt and Y. Winter. Energetic cost of hovering flight in nectar-feeding bats (phyllostomidae : Glossophaginae) and its scaling in moths, birds and bats. *Journal of Comparative Physiology B-Biochemical Systemic and Environmental Physiology*, 169(1):38–48, 1999.

[34] D. Warrick, B. Tobalske, and D. Powers. Aerodynamics of the hovering hummingbird. *Nature*, 435(7045):1094–1097, 2005.

[35] D. Willis, J. Peraire, and J. White. A combined pFFT-multipole tree code, unsteady panel method with vortex particle wakes. *Int. J. for Numerical Methods in Fluids*, 53(8):1399, 2007.

[36] D. J. Willis, D. K. Riskin, K. S. Breuer, S. M. Swartz, and J. Peraire. Computational modeling of the aeromechanics of a bat, cynopterus brachyotis, based on high resolution, experimentally recorded kinematics: Part i – a description of the computational models. *J. Exp. Bio.*, 2008. In Review.

[37] A. Willmott, C. Ellington, and A. Thomas. Flow visualization and unsteady aerodynamics in the flight of the hawkmoth, manduca sexta. *Philosophical Transactions of the Royal Society of London Series B-Biological Sciences*, 352(1351):303–316, 1997.

[38] Y. Winter, C. Voigt, and O. V. Helversen. Gas exchange during hovering flight in a nectar-feeding bat glossophaga soricina. *Journal of Experimental Biology*, 201(2):237–244, 1998.

[39] H. Zhou, M. Chen, and M. F. Webster. Comparative evaluation of visualization and experimental results using image comparison metrics. In *Proc. of Visualization '02*, pages 315–322, 2002.

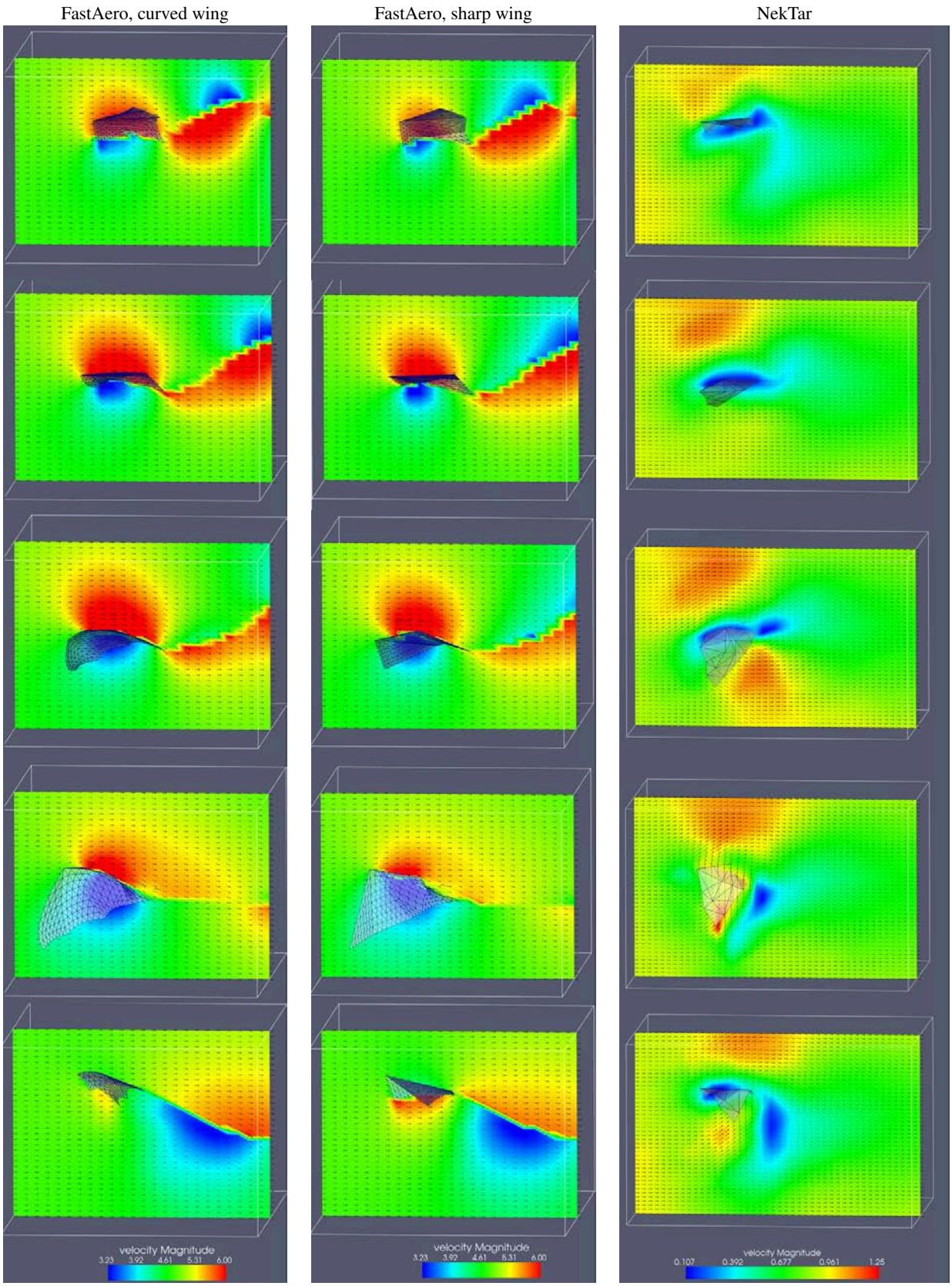

Fig. 9. v_{BFR}, FastAero and NekTar: Absolute velocity field in a spanwise slicing plane during downstroke and upstroke. In NekTar, the viscous effects force the flow to go slower at the surface of the wing, but this behavior is not seen in the FastAero cases. Since Re of the NekTar simulation is very low, the viscous effects are strongly manifested in the appearance of wide boundary layers.

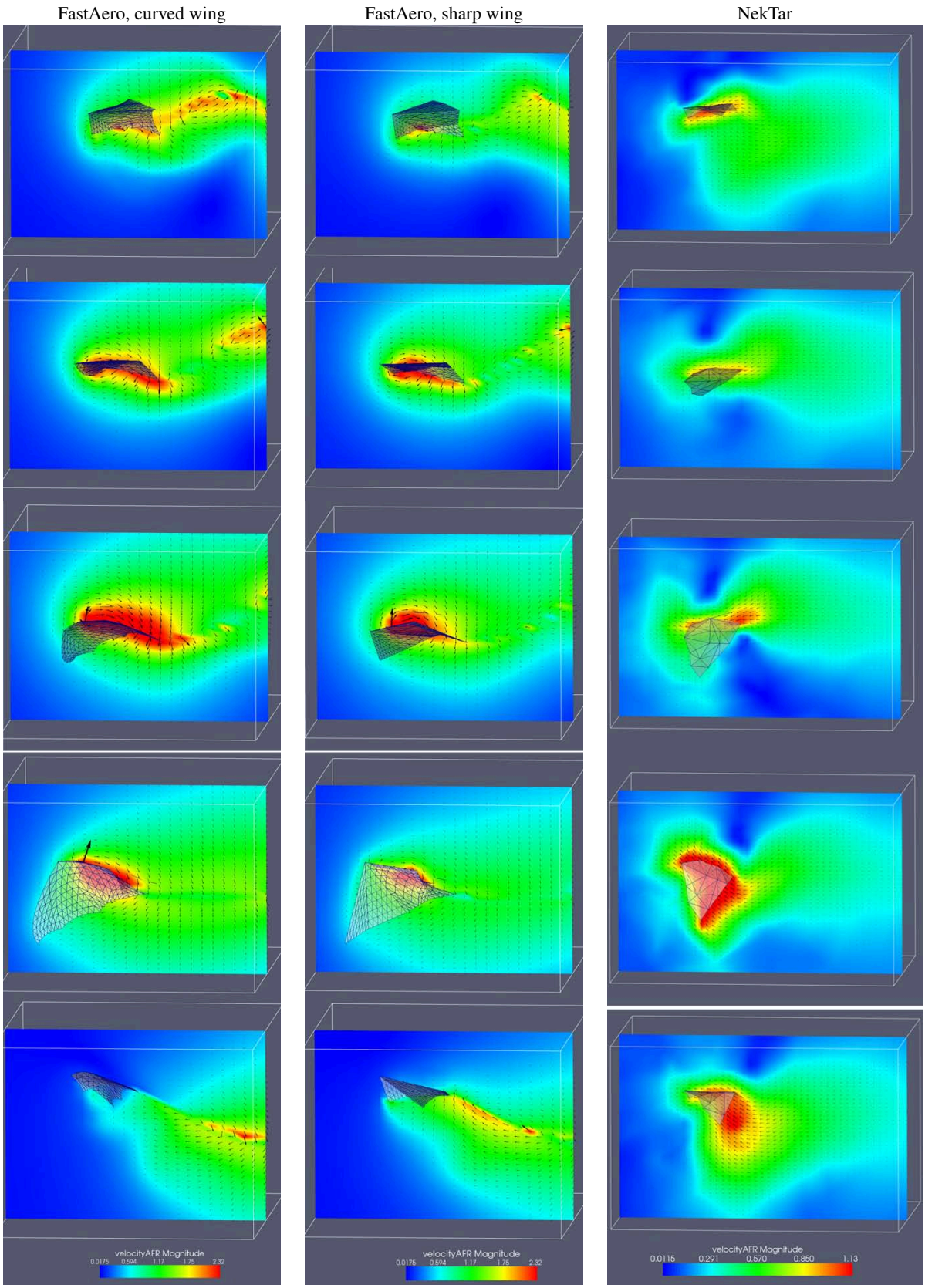

Fig. 10. v_{AFR}, FastAero and NekTar: Absolute velocity field in the mid-wing spanwise slicing plane during downstroke and upstroke. Viscous effects in NekTar are reflected in the behavior of the high v_{AFR} magnitude region, as the disturbance is manifested close to the wing surface. In FastAero, on the other hand, these regions are continuously shed from the wing.

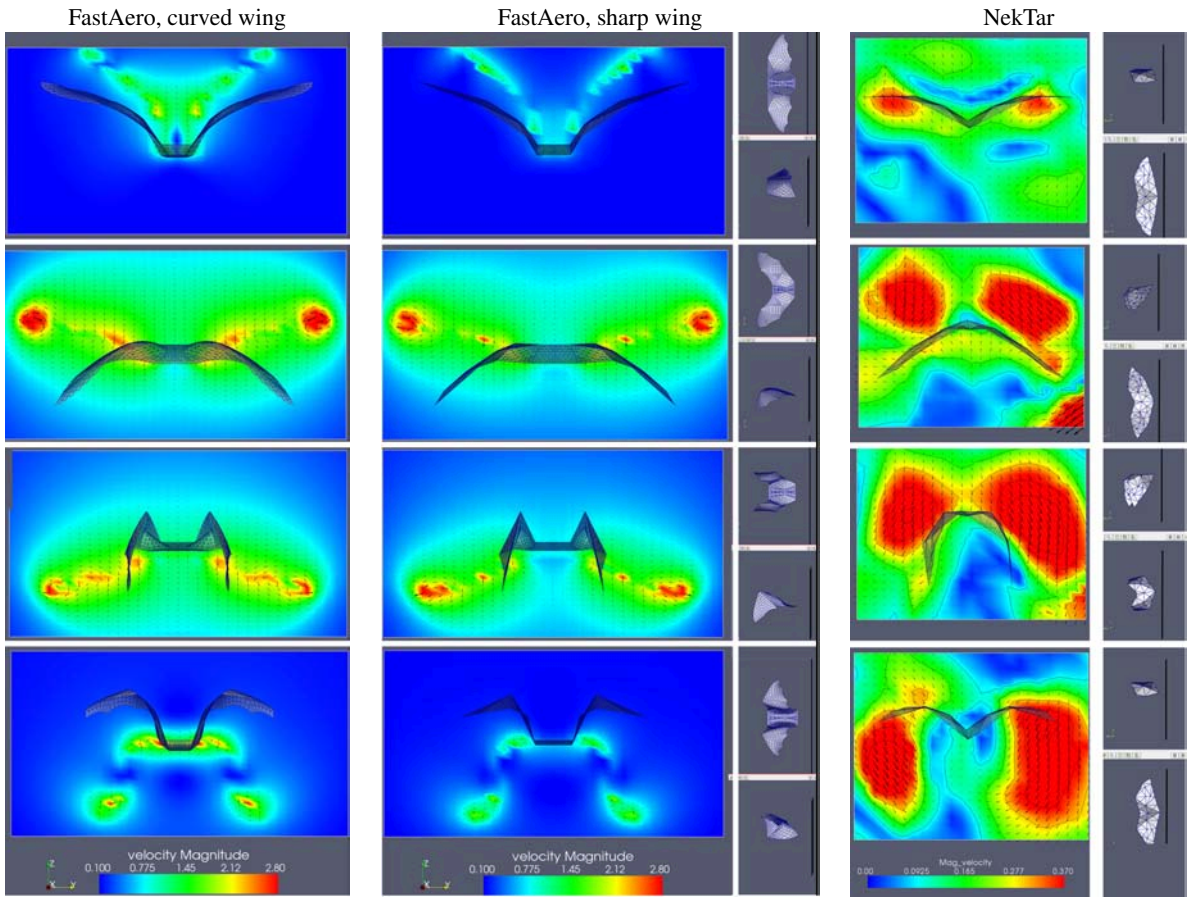

Fig. 11. FastAero and NekTar: Absolute velocity field in the transverse v_{BFR} plane behind the bat during downstroke and upstroke, for all three cases. The changing shape of the wing and the relative position of the cutting plane is shown on the right. In the two FastAero cases, the curved wing case higher magnitude wake velocities seem more smeared, whereas in the sharp wing case higher magnitude velocity appears more localized in the regions near joints. In the NekTar case, the two large trailing vortices are fairly stable due to the effects of viscosity. The NekTar field is asymmetric because of the preprocessing step – when mirroring the wing geometry, the body axis was not constrained to the constant direction of flight, so there is a slight yaw.